Article

Material evaluation and dynamic powder deposition modeling of PEEK/CF composite for powder-bed fusion process

Jiang Li [1*], Fulun Peng [1*], Hongguang Li [1], Zhibing Ru [1], Junjie Fu [1] and Wen Zhu [2]

[1] Xi'an Institute of Applied Optics, Structure Department of Reconnaissance Vehicle R&D Center，Xi'an 710065, Shaanxi, China

[2] State IJR Center of Aerospace Design and Additive Manufacturing, Northwestern Polytechnical University, 710072 Xi'an, China

* Correspondence: lijiang235@163.com (J.L.); pcoolfy@163.com (F.P.); Tel.: +86-177-9160-5573 (J.L.); +86-189-9120-5818 (F.P.)

Abstract: Polymeric composites such as Poly-ether-ether-ketone (PEEK)/carbon fiber (CF) have been widely utilized due to outstanding performances such as high specific strength and specific modulus. The PEEK/CF components via powder-bed fusion additive manufacturing usually show brittle fracture behaviors induced by their poor interfacial affinity and inner voids. These defects are strongly associated with powder packing quality upon deposition. The particle dynamic model has been widely employed to study the interactions of particle motions. Powder property, bulk material property, and interfacial features of composite powders are key factors in the particle dynamic model. In this work, an efficient and systematic material evaluation is developed for composite powders to investigate their deposition mechanism. The discrete element method is utilized to simulate the dynamic behaviors of PEEK/CF composite powders. The powder properties, bulk material properties, and interfacial features of powders are calibrated and justified by experimental measurement, numerical simulation, and design of experiments. The particle dynamic model can well explain the powder flow behaviors and interactions. It reveals that the addition of short CF particles can assist the flow of PEEK powders and improve the packing quality of the composite powders.

Keywords: Powder-bed fusion; Composite polymers; Discrete element method; Material characterization; Additive manufacturing.

1. Introduction

Selective laser sintering, as an essential category of multiple additive manufacturing technologies, is able to produce polymeric composite materials economically and with obvious flexibility [1]. Polymeric composites such as Poly-ether-ether-ketone (PEEK)/carbon fiber (CF) have attracted the attention of researchers as well as industrialists due to outstanding performances such as high specific strength and specific modulus. However, the laser-sintered PEEK/CF components are usually brittle because of their poor interfacial affinity, and inner voids. These defects are strongly associated with the powder packing quality upon deposition. Thus, the investigation of the powder deposition process incorporating the detailed material properties is necessary, so that the expected behaviors of the laser-sintered PEEK/CF composites can be achieved.

The particle dynamic model has been widely employed to study the interactions between particles in macro-scale or micro-scale, especially the powder deposition process [2, 3]. The powder property, bulk material property, and interfacial features of composite powders are key factors influencing the packing quality of deposited layers in the powder-bed fusion (PBF) process. Thus, the detailed material evaluation for the dynamic model is significant to reveal the deposition mechanism of composite powders. The evaluation of specific materials has been carried out, such as agriculture [4-6], soil [7, 8], and rock [9-11]. However, little research has conducted the raw material evaluation correlating with the polymer and polymer-based composite powders. Opposite to the pure materials,

 doi:10.20944/preprints202306.0607.v1

the multi-component composite powders will improve the quantities of to-be-determined constants. It also brings some parameters that cannot be measured directly, such as surface energy.

When exploring these specific properties, the reliable approach is to perform either in-situ measurements or laboratory experiments. Vu-Quoc et al. [12] measured the restitution coefficient in soybeans by conducting drop tests from various heights. They used the data from high-speed video to determine the final parameters. Marczewska et al. [13] utilized the triaxial test to investigate the effects of particle-particle sliding friction and contact stiffness, including Young's modulus, Poisson's ratio, and dilatancy. Other experimental measurements such as uniaxial tension, slope test, direct shear test, etc…also play an important role. However, it is difficult to measure the specific contact parameters in CF-reinforced composite powders. Since preparing the pure CF sample is a struggle, causing inconvenience in the corresponding experiments. Thus, it is appropriate to compute the specific coefficient by the finite element simulation in macro-scale. Some parameters can not be measured by experiments such as surface energy, which can be determined by the design of experiments (DOE) method. Yoon et al. [9] employed the response surface method and the Plackett-Burman (PB) design to acquire suitable parameters to simulate the uniaxial compression of bonded rock. Johnstone [14] used the DOE method to calibrate the dynamics model based on experimental measurements. E. X. Zu et al. [15] carried out the simulation of coke accumulation based on the Hertz-Mindlin (no-slip) contact model. The core of their study is to determine the contact parameters. The number of investigated factors has a great influence on the complexity of the DOE. So the number of studied factors should be reduced as much as possible especially for the composite powders. Moreover, the multi-phase characteristics of polymer composite powders significantly increase the number of undetermined parameters, causing difficulties in calibrating the DEM parameters. Thus, this work proposes a parameter design method called "Plackett Burman (PB)-Box Behnken design (BBD)-Genetic Algorithm (GA)" for the DEM model parameter calibration process. This method mainly aims at contact parameters that are difficult to measure experimentally. It can quickly obtain the functional relationship between the significant parameters and the target value, and determine the optimal parameter combination. Importantly, this method possesses universality for multi-phase powder systems.

In this work, to develop a reliable powder dynamics model for powder deposition in PBF, a systematic framework for material evaluation of PEEK/CF powders with different compositions is proposed. Therein, the powder properties, bulk material properties, and interfacial features are calibrated by experimental measurement, numerical simulation, and DOE method. The powder dynamics model for PEEK/CF powders is experimentally verified by the fluidity-reflected angle of repose (AOR). Ultimately, the powder deposition processes of PEEK and PEEK/CF powders are evaluated and analyzed through the experiments and the validated dynamics model.

2. Discrete element method

2.1 Contact model theory

The discrete element method (DEM) is utilized to simulate the dynamic behaviors of PEEK/CF composite powders. In the DEM simulation, the particles are modeled as discrete entities to describe the dynamics of particle flow. The translation, rotation, and location of the particles can be characterized by Newton's laws of motion, which is described as [16, 17]:

$$m_i \frac{dv_i}{dt} = \sum F_{c,i} + m_i g \tag{1}$$

$$\frac{d\left(I_i \cdot \omega_i\right)}{dt} = R_i \cdot \sum M_{c,i} \tag{2}$$

Preprints (www.preprints.org) | NOT PEER-REVIEWED | Posted: 8 June 2023 doi:10.20944/preprints202306.0607.v1

where m_i, ω_i, v_i, I_i are the mass, angular velocity, translational velocity, and moment of inertia, respectively. $F_{c,i}$ is the contact force, $M_{c,i}$ is the contact torque, R_i is the rotation matrix.

The relationship between cohesive force and particle size is shown in Figure 1(a) [18, 19]. It appears that the cohesive forces such as Van der Waals force, electrostatic force, and capillary force are greater than the gravity of particles when the particle size is less than 100 μm, which reduces the powder fluidity and makes inconvenience for the powder-spreading process. In reality, the powder is preheated and dried before the powder-spreading process. Thus, the capillary force can be ignored.

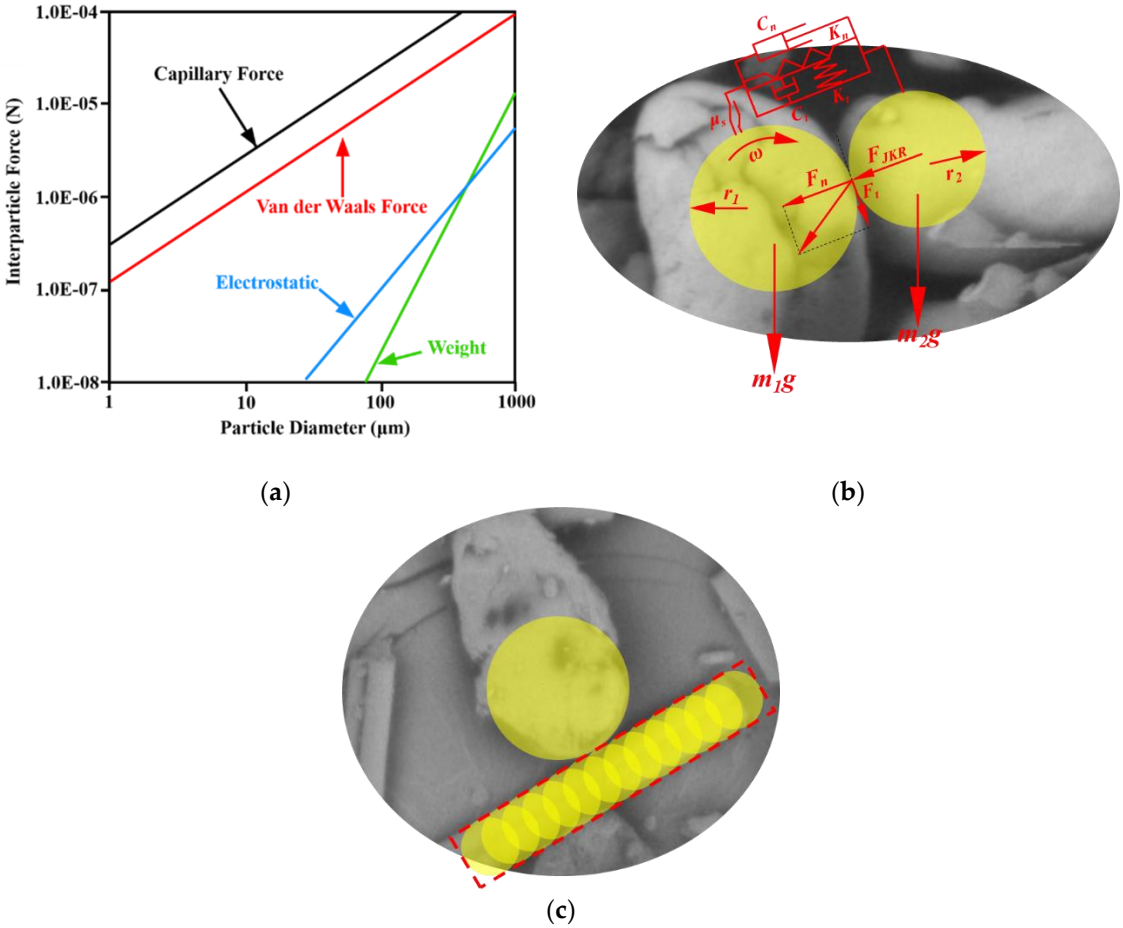

Figure 1. Interaction between particles and particle modeling method: (**a**) The relationship between particle force and particle diameter [18]; (**b**) Contact force diagram between particles; (**c**) Multiple-sphere method to model the CF particle.

(1) Hertz-Mindlin contact model

The rationality of the Hertz-Mindlin contact model has been widely recognized in the particle-related research field [20, 21]. In order to accurately characterize the stress-strain relationship between particles considering the adhesion, this work adopts Hertz-Mindlin and Johnson Kendall Roberts (JKR) model for polymers and their composite powders, which is implemented using EDEM software. Among them, the Hertz-Mindlin model is the foundation of the DEM method, and the parameter of surface energy in the JKR model can comprehensively characterize the bonding effect between particles caused by the van der Waals force and the electrostatic force [22]. Therefore, the Hertz Mindlin and JKR models possess universality in the DEM simulation of other thermoplastic polymers and their composite powders.

In the Hertz-Mindlin model, the normal and tangential force components between particles are calculated based on the Hertzian contact theory and the Middlein-

Preprints (www.preprints.org) | NOT PEER-REVIEWED | Posted: 8 June 2023 doi:10.20944/preprints202306.0607.v1

Deresiewicz method respectively [23, 24]. Both normal and tangential force between particles have damping components. The damping coefficient is related to the restitution coefficient [25].The tangential friction force between particles follows the Coulomb's law of friction, and the rolling friction between particles is computed based on the Contact-Directional-Constant-Torque model [17, 26].

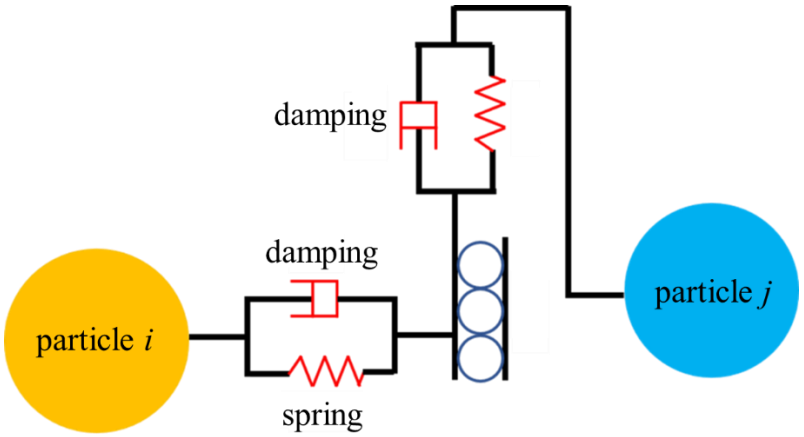

Figure 2. Hertz-Mindlin contact model.

Figure 2 shows the schematic diagram of the Hertz Mindlin model for adjacent particles *i* and *j*, where the normal contact force on particle i can be expressed as

$$F_{CN}=F_{CN,E}+F_{CN,D} \tag{3}$$

where $\boldsymbol{F}_{CN,E}$ is the normal elastic force, $\boldsymbol{F}_{CN,D}$ is the normal damping force. The $\boldsymbol{F}_{CN,E}$ is computed based on the Hertz contact theory, which is described as

$$F_{CN,E}=-K_n\times\alpha_n^{1.5} \tag{4}$$

where $\boldsymbol{\alpha}_n$ is the normal contact displacement (overlap of adjacent particles). The Contact constant K_n is expressed as

$$K_n=\frac{4G\sqrt{r^*}}{3(1-\upsilon)} \tag{5}$$

where G is the shear modulus of the particle. r^* is the radius of the local curvature. υ is the Poisson's ratio.

The normal damping force $\boldsymbol{F}_{CN,D}$ between particles is expressed as

$$F_{CN,D}=-2\sqrt{\frac{5}{6}}\beta^*\sqrt{m^*\times k_n}\times v_{re,n} \tag{6}$$

where $\boldsymbol{v}_{re,n}$ is the component of the relative velocity of particle i relative to particle j along the normal direction. k_n is the normal contact stiffness, β^* is the damping coefficient, m^* is the equivalent mass. Therein, the damping coefficient and normal contact stiffness can be expressed as

$$\beta^*=\frac{\ln e}{\sqrt{\ln^2 e+\pi^2}} \tag{7}$$

$$k_n=\frac{2G}{1-\upsilon}\left(\frac{3(1-\upsilon)\times r^*\times F_{CN,E}}{4G}\right)^{\frac{1}{3}} \tag{8}$$

Preprints (www.preprints.org) | NOT PEER-REVIEWED | Posted: 8 June 2023 doi:10.20944/preprints202306.0607.v1

where e is the restitution coefficient between particles. The equivalent mass m^* and equivalent curvature radius r^* of particles are respectively described as

$$m^* = \frac{m_i \times m_j}{m_i + m_j} \tag{9}$$

$$r^* = \frac{r_i \times r_j}{r_i + r_j} \tag{10}$$

where m_i and m_j represent the masses of adjacent particles i and j. r_i and r_j are the radiuses of adjacent particles i and j.

The tangential contact force $\boldsymbol{F}_{CT}$ between adjacent particles can be expressed as

$$F_{CT} = F_{CT,E} + F_{CT,D} \tag{11}$$

where $\boldsymbol{F}_{CT,E}$ is the elastic force along the tangential direction, $\boldsymbol{F}_{CT,D}$ is the damping force along the tangential direction. The tangential elastic force $\boldsymbol{F}_{CT,E}$, can be expressed in incremental form as

$$F_{CT,E} = F_{CT,E,(n-1)} + \Delta F_{CT,E} \tag{12}$$

where $\boldsymbol{F}_{CT,E,(n-1)}$ is the tangential elastic force of the previous analysis step; $\Delta\boldsymbol{F}_{CT,E}$ is the increment of the tangential elastic force in the current analysis step, which is described as

$$\Delta F_{CT,E} = k_t \times \Delta\alpha_t \tag{13}$$

where $\Delta\boldsymbol{\alpha}_t$ is the tangential displacement increment, k_t is the tangential spring stiffness, and expressed as

$$\Delta\alpha_t = v_{re,t} \times \Delta t \tag{14}$$

$$k_t = \frac{2}{2-v}\left(6(1-v) \times G^2 \times r^* \times F_{CN,E}\right)^{\frac{1}{3}} \tag{15}$$

where $\boldsymbol{v}_{re,t}$ is the relative tangential velocity between particles, Δt is the step time. Meanwhile, the tangential damping force between adjacent particles can be expressed as

$$\Delta F_{CT,D} = -2\sqrt{\frac{5}{6}} \times \beta^* \times \sqrt{m^* \times k_t} \times v_{re,t} \tag{16}$$

It is worth noting that the tangential force between adjacent particles is related to the frictional force between particles ($\mu_s\boldsymbol{F}_{CN}$, μ_s is the static friction coefficient). In the simulation process, the rolling friction can not be ignored, which is achieved by applying a torque to the contact surface of the particles.

$$\tau_i = -\mu_r F_{CN} R_i \omega_i \tag{17}$$

where R_i is the distance from the contact point to the mass center, μ_r is the rolling friction coefficient, $\boldsymbol{\omega}_i$ is the unit angular velocity vector at the contact point.

(2) JKR theory

The Hertz Mindlin with JKR contact model can form an adhesive force contact model between particles, mainly considering the influence of van der Waals forces in the contact area. In this model, the normal elastic contact force between particles is computed based on the JKR theory [27], including the overlap of particles δ, interaction parameters, and surface energy γ, which can be described as

Preprints (www.preprints.org) | NOT PEER-REVIEWED | Posted: 8 June 2023 doi:10.20944/preprints202306.0607.v1

$$F_{JKR}=-4\sqrt{\pi\gamma E^*}\alpha^{\frac{3}{2}}+\frac{4E^*}{3r^*}\alpha^3 \tag{18}$$

$$\delta=\frac{\alpha^2}{r^*}-\sqrt{\frac{4\pi\gamma\alpha}{E^*}} \tag{19}$$

$$\frac{1}{E^*}=\frac{\left(1-v_i^2\right)}{E_i}+\frac{\left(1-v_j^2\right)}{E_j} \tag{20}$$

where E^* is the equivalent Young's modulus, r^* is the equivalent curvature radius, α is the contact radius of particles.

It is discovered that several parameters are involved in the aforementioned model, such as static friction coefficient, rolling friction coefficient, restitution coefficient, and surface energy. Therefore, it is essential to carry out the parameter-calibration work through the material characterization.

2.2 Parameter classification of the Discrete Element Model

The first step of the DEM simulation is to calibrate numerous parameters through the comprehensive material characterization. Figure 3 shows the parameters involved in the DEM model, which can be divided into three categories.

(1) Solid-phase parameters: solid phase density, elastic modulus, and Poisson's ratio;

(2) Contact parameters between particles: static friction coefficient, rolling friction coefficient, restitution coefficient, and surface energy.

(3) Powder-phase parameters: particle morphology, particle size, and powder fluidity.

For composite powders, the contact forms between particles can be further divided into three patterns of "particle-particle", "particle-reinforced phase", and "reinforced phase- reinforced phase". Specifically, the particle size and the static friction coefficient between particles are directly measured. The restitution coefficient is obtained by the FEM simulation. The rolling friction coefficient and surface energy are achieved by the "PB-BBD-GA" parameter-design method. This method extends the GA on the basis of traditional PB and BBD methods, avoiding the uncertainty of traditional methods in predicting the optimal parameter combination. The "PB-BBD-GA" method can quickly obtain the functional relationship between significant parameters and target values, and determine the unknown parameter combination more accurately and efficiently.

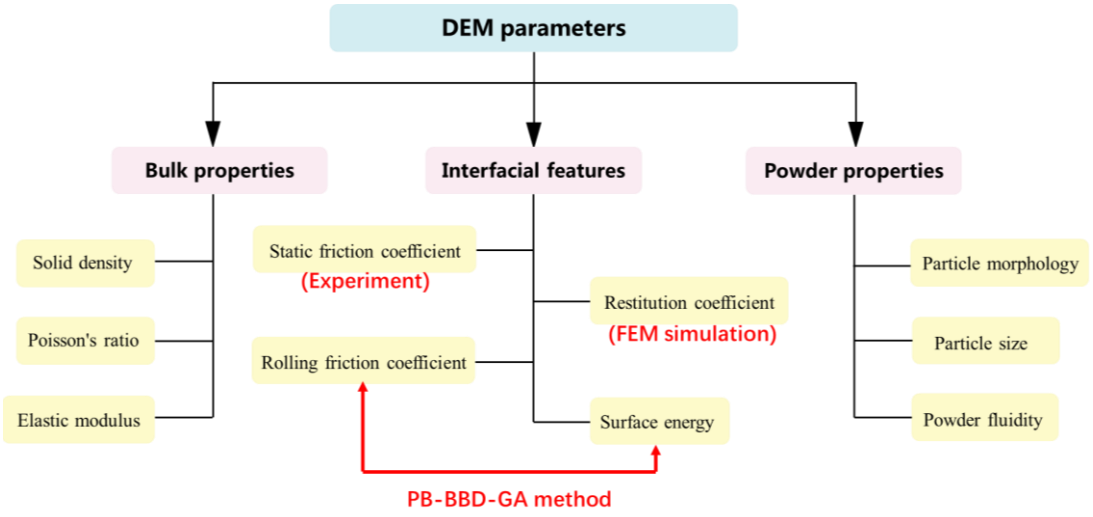

Preprints (www.preprints.org) | NOT PEER-REVIEWED | Posted: 8 June 2023 doi:10.20944/preprints202306.0607.v1

Figure 3. Parameter classification and calibration methods of the DEM model.

2.3 Analysis step and particle modeling

The DEM simulation is proceeding based on the time step. In the numerical computation, a differential equation needs to be transformed into a difference equation for the iterative solution. The time step is the time difference between two adjacent iterations. The time step is usually set to 20%-30% of Rayleigh time, which makes the simulation stable and time-saving. Rayleigh time is determined as [28]

$$T_R = 1.625 R_{min} \sqrt{\frac{\rho}{E}} \tag{21}$$

where R_{min} is the minimum radius of spherical members and ρ is the density. In this work, the Rayleigh time is 6.4175e-9 s and the DEM results are recorded every 0.001 s.

The particle model is established based on its morphology in the DEM simulation, and the spherical particles are computationally efficient compared with the non-spherical particles. Importantly, the contact model for spherical particles should include rolling resistance to model the rotational motion of actual non-spherical particles. In contrast, the rolling resistance can be omitted when utilizing the non-spherical particles [29]. In this work, the spherical particles are modeled and the rolling resistance represented by the rolling friction coefficient is determined lastly. Meanwhile, a multi-sphere method, by which multiple spheres with the same or different sizes are clumped to approximate the irregularly-shaped particle (such as CF in this work), is employed in the model [30], as shown in Figure 1(c).

3. Material and the experimental method

3.1 Material characterization

This work selects the materials of PEEK and PEEK/CF powders, which possess the features of poor powder fluidity and high difficulty in powder deposition process, as the representative research object. The adopted powders are the PEEK, PEEK/CF_30wt%, and PEEK/CF_50wt%, which are featured by the weight fraction of CF. The inherent properties of the compositions of PEEK and CF are listed in Table 1, which includes important input factors of the subsequent-introduced powder dynamics model.

Table 1. The inherent mechanical properties of PEEK, CF, and the glass.

Material	Elastic modulus (Gpa)	Poisson ratio	Density (kg/m³)	Reference
PEEK	3.6	0.38	1300	[31]
CF[1]	15	0.2	1760	[32]
Glass	64	0.2	2230	ISO 3585-1998

[1] Elastic modulus of CF is 15Gpa along the horizontal direction.

As shown in Figure 3, a large number of constants need to be determined, which are detailly described as follows.

(1) Angle of repose

Powder fluidity is a comprehensive characterization and deeply impacts the powder deposition process. The AOR can reflect the powder fluidity in a simple and convenient fashion. In this paper, the AOR is measured according to the GB11986-89. As shown in Figure 4, a funnel is fixed above the horizontal plate, through which the particle sample falls, and the AOR of the cone is measured. Both experiments and the DEM model follow this standard.

 doi:10.20944/preprints202306.0607.v1

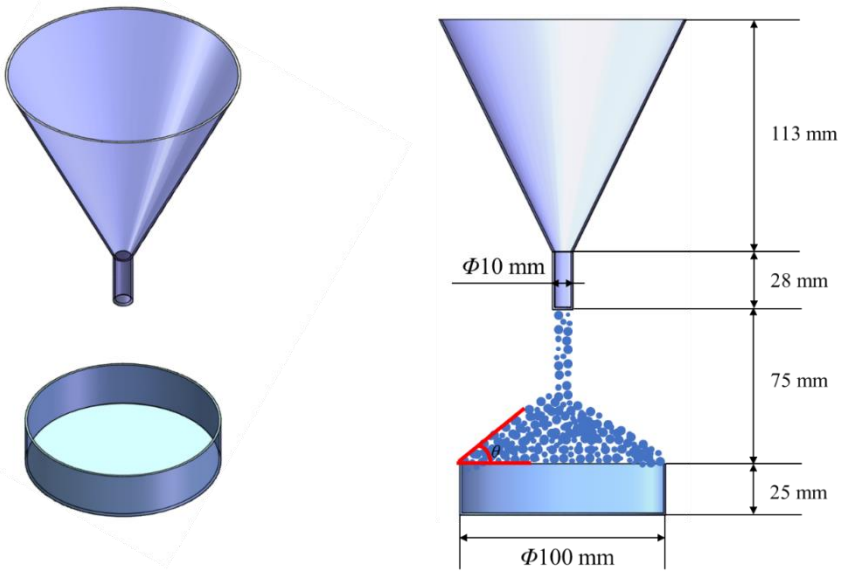

Figure 4. The AOR experiment according to the GB11986-89.

(2) Particle morphology and particle size distribution

Particle morphology and particle size distribution have important impacts on powder fluidity and computational efficiency. The TM4000PLUS scanning electron microscope (SEM) equipment is utilized in the high vacuum circumstance and at a voltage of 5 kV to acquire the SEM images that characterized the morphological features of PEEK powders and PEEK/CF composite powders. The objective area of the SEM image is limited. So the Malvern laser particle sizer (Mastersizer 2000, the United Kingdom) is utilized to measure the accurate particle size distribution of PEEK and CF.

(3) Bulk density

The measurement method for the bulk density of PEEK and PEEK/CF powders is shown in Figure 5. Prepare a 100 ml graduated cylinder, and place the funnel at a certain height directly above the cylinder. The powder falls freely from the funnel mouth and fills the cylinder. Thereafter, screed the surface of the graduated cylinder, place it on the electronic scale to measure its mass, and obtain the bulk density of the powders ultimately.

Preprints (www.preprints.org) | NOT PEER-REVIEWED | Posted: 8 June 2023 doi:10.20944/preprints202306.0607.v1

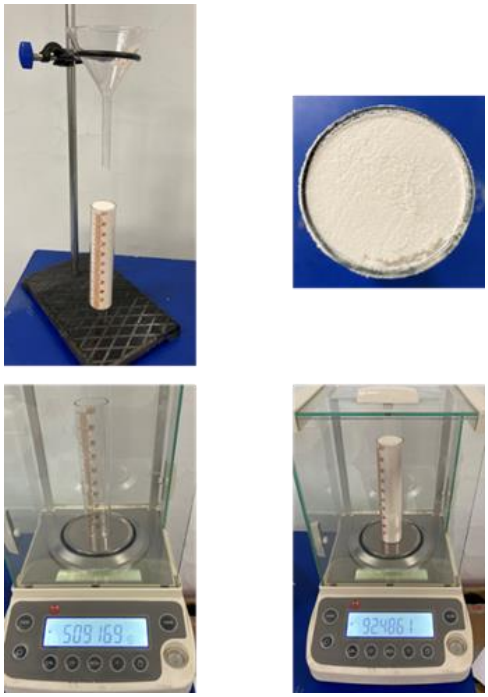

Figure 5. Measurement for the bulk density.

(4) Static friction coefficient

The inclined plane test can be used to measure the static friction coefficient. The friction coefficient between different materials can be achieved by replacing the material of the inclined plane or sample. At first, the inclined plane is placed horizontally, and the sample is placed at the fixed position of the inclined plane. Then lift the slope slowly, and stop the inclined plane when the sample starts to slide. The position of the inclined plane at this moment is recorded through a camera and the tilt angle is read. The static friction coefficient is the tangent value of the inclination angle.

(5) Restitution coefficient

The restitution coefficient is the ratio of the separation velocity and the approaching velocity of the two objects along the normal direction of the contact before and after the collision, which is only related to the material of the collision objects [33]. Generally, it can be experimentally measured. Fix the plate, and a ball falls freely above the plate. The coefficient of restitution can be calculated by recording the fall height and bounce height of the ball (the restitution coefficient between different materials is achieved by changing the materials of the plate and the free-falling ball). However, measuring the restitution coefficient associated with pure CF is a struggle due to the difficulty in producing the products in pure CF in reality. Thus, it is appropriate to calculate the restitution coefficient by the simulation. The process of free-falling and bouncing for a small ball is achieved by FEM simulation (as shown in Figure 6) [34]. The restitution coefficient is computed as

$$e = \frac{v_{off}}{v_{app}} \tag{22}$$

where v_{app} is the speed of the ball approaching the plate, v_{off} is the speed of the ball away from the plate. e denotes the restitution coefficient.

Preprints (www.preprints.org) | NOT PEER-REVIEWED | Posted: 8 June 2023 doi:10.20944/preprints202306.0607.v1

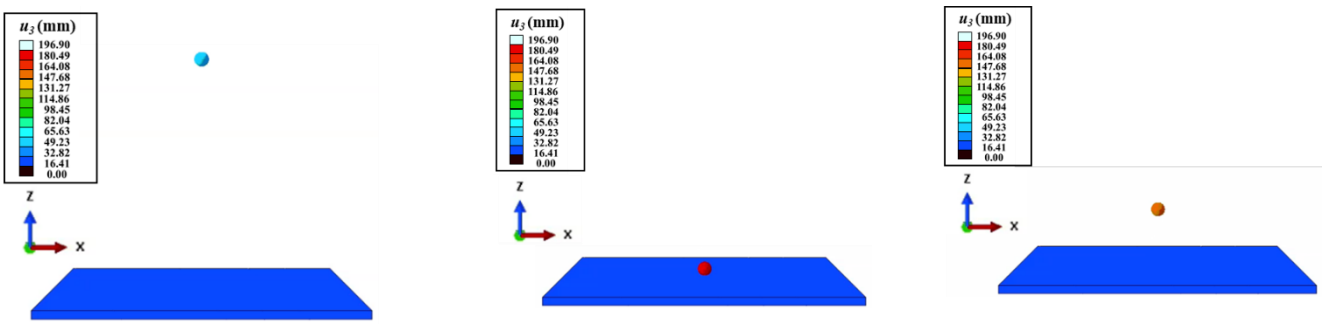

(**a**) (**b**) (**c**)

Figure 6. FEM simulation of the restitution coefficient: (**a**) Initial moment; (**b**) Contact with bottom plate; (**c**) Bouncing to maximum height.

(6) Rolling friction coefficient and surface energy

Experimentally measuring the rolling friction coefficient and surface energy is a struggle even impossible to achieve. Thus, the DOE including the PB, BBD, and GA is employed to determine them.

PB design is a two-level (-1 and +1) experimental design method, which attempts to screen and determine the factors that significantly impact the results with the least number of trials. In this work, AOR is used as the response value to screen eight factors corresponding to the powders of PEEK/CF_30wt%. These factors with their initial parameter spaces are listed in Table 2. When determining the parameter space, the ratio of high and low levels of the two parameters is set to be identical in order to prevent significance fluctuation between the investigated factors [35]. The detailed design and results of the PB design are discussed in Section 4.2.

Table 2. The parameters of the PB test.

Parameters	Symbol	Initial parameter space
PEEK-PEEK rolling friction	X_0	
PEEK-CF rolling friction	X_1	
CF-CF rolling friction	X_2	0.01-0.2
PEEK-glass rolling friction	X_3	
CF-glass rolling friction	X_4	
PEEK-PEEK surface energy	X_5	
PEEK-CF surface energy	X_6	0.001-0.02 (J/m²)
CF-CF surface energy	X_7	

The BBD design is utilized to further investigate the optimal points of the key factors based on the PB results. The computed results are analyzed afterward by the response surface method. The corresponding variables are coded as follows:

$$X_i=(x_i-x_0)/\Delta x_i \quad (i=1,2,...,k) \tag{23}$$

where X_i is the coded value of the independent factor, x_0 is the real value at the center point, x_i is the real value, and Δx_i is the value of step-change.

The BBD model can be described by the quadratic equation:

$$Y=\beta_0+\sum\beta_i X_i+\sum\beta_{ii}X_i^2+\sum\beta_{ij}X_iX_j \quad (i=1,2,...,k) \tag{24}$$

where Y is the predicted response value (AOR in this work). X_i and X_j are the coded independent variables. β_0 is the offset term, β_i is the linear term, β_{ii} is the squared term, and β_{ij} is the interaction term.

GA is developed by imitating the mechanism of natural biological evolution. It is an efficient, parallel, global searching method, which can automatically acquire and

Preprints (www.preprints.org) | NOT PEER-REVIEWED | Posted: 8 June 2023 doi:10.20944/preprints202306.0607.v1

accumulate knowledge about the searching space, and the searching process is adaptively controlled to obtain the optimal solution. The entire GA is achieved based on the Matlab GA toolbox in this work.

3.2 Powder deposition process

The reliability of the complete model is supposed to be experimentally verified. The comprehensive indicator AOR can be used as the target, which reflects the overall performance of the studied powder. In addition, this work investigates the effect of CF on the surface properties of the deposited powder layer through powder deposition experiments (similar to the scraper form of the actual PBF process) and corresponding simulation.

The surface roughness is the key factor in the powder deposition process. It has a great influence on the sintering process and the subsequent recoating process. Thus, it is necessary to investigate powder deposition through the powder dynamics model. By comparing with the corresponding experiment, the powder dynamics model can be further verified by this practical application.

The powder deposition is experimentally conducted based on a piece of slotted glass, which is shown in Figure 7(a). The preparation steps are proceeded as follows: (1) Prepare a piece of glass with a groove of 0.8-1 mm; (2) load enough powder manually in front of the groove; (3) use another piece of glass to scrape the loaded powders slowly from left to right with a tilt angle of around 45°; (4) the surface of the powders in the groove is smooth with the naked eye as shown in Figure 7(b); (5) The surface morphology of the target zones (Figure 7(c)) is measured by a microscope (J6000, Keyence, Shanghai, China). The observed area is located at the center of the powder layer.

In the DEM model, set the same conditions as the experiment. When the simulation of the powder deposition process is completed, obtain the surface particle contour curve at the center of the powder layer (as shown in Figure 7(d)). The fluctuation of the contour curve reflects the flatness of the powder surface.

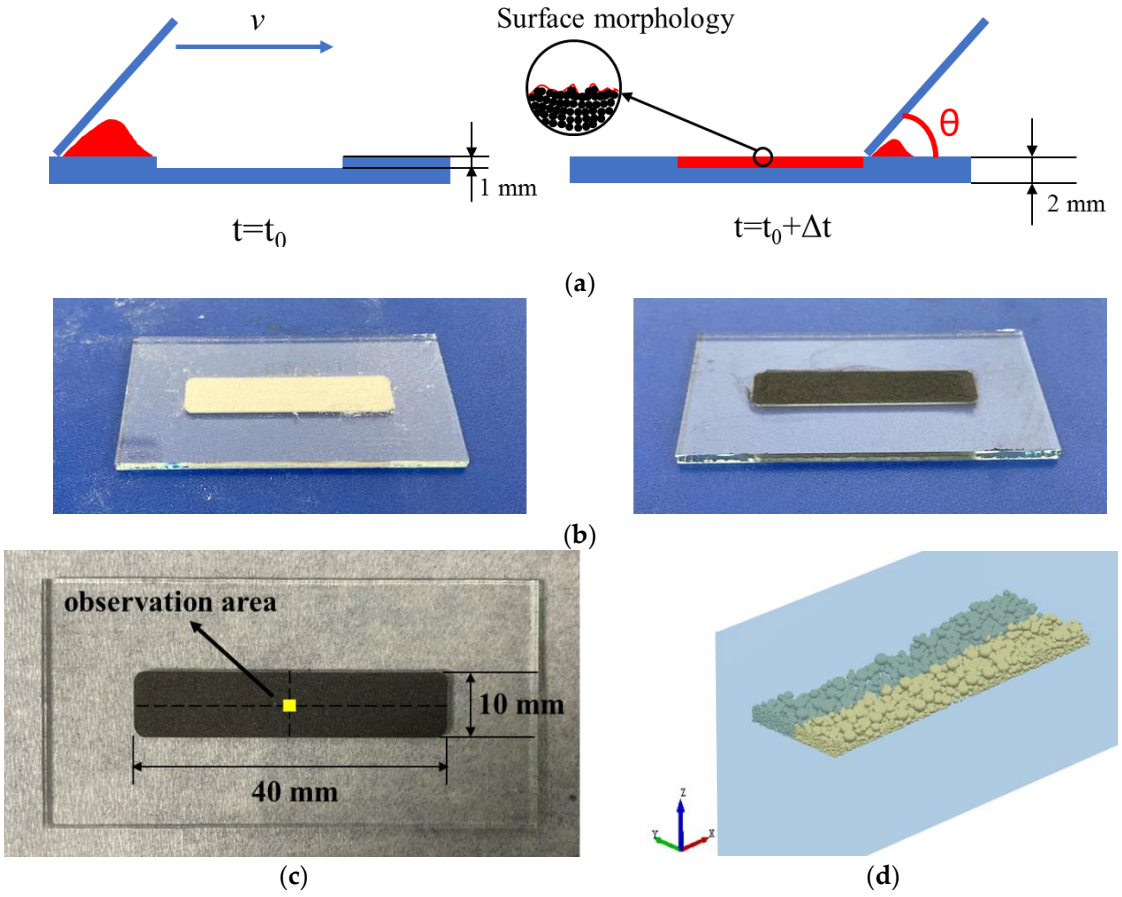

Preprints (www.preprints.org) | NOT PEER-REVIEWED | Posted: 8 June 2023 doi:10.20944/preprints202306.0607.v1

Figure 7. The powder deposition process of experiment and simulation: (**a**) The powder deposition process and the surface morphology observation; (**b**) The flat surface of the spread powder with the naked eye; (**c**) The observation zone; (**d**) The cross-section position of the simulated powder layer.

4. Results and discussion

This section firstly describes the material properties of PEEK and PEEK/CF in detail, including the particle morphology, particle size, and AOR, determines the contact parameters between particles (such as rolling friction coefficient, restitution coefficient, and surface energy), and experimentally verifies the reliability of the determined parameters. Secondly, the powder deposition process is investigated through the experiment and the DEM simulation. The influence of CF particles on the surface performance of the powder deposition layer is analyzed.

4.1 Material evaluation

The particle size distribution is obtained as input information in DEM, and it significantly influences the computational efficiency. The SEM pictures of pure PEEK and PEEK/CF_30wt % are given in the following Figure 8. It shows that powder particles of PEEK are almost ellipsoidal. The diameter of CF is uniform, but the length distribution is obviously dispersed. To specifically characterize the particle size information, the powders of PEEK and CF are detected through the laser particle sizer and the results are given in Table 3 and Figure 9.

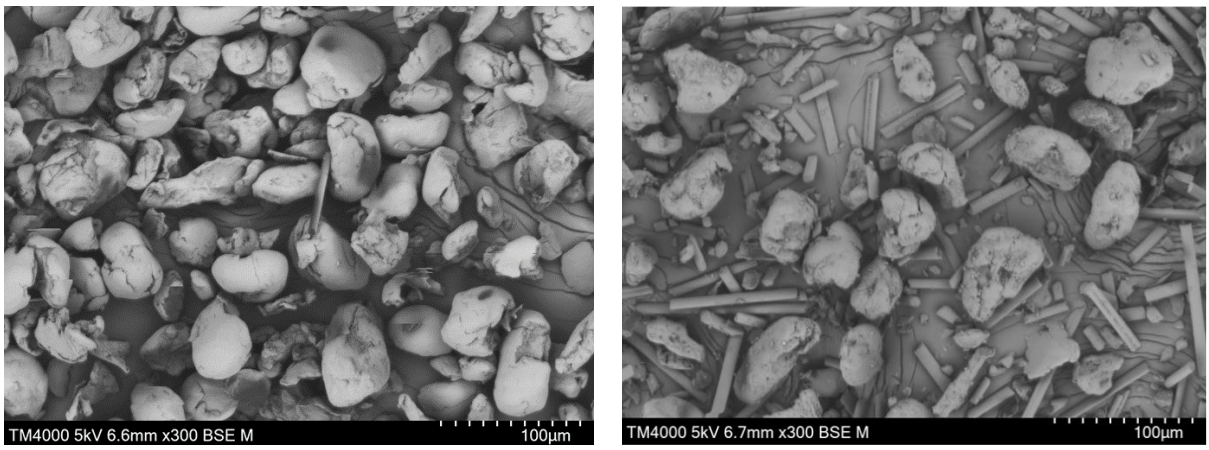

(**a**) (**b**)

Figure 8. The results of SEM experiments: (**a**) Particle morphology of PEEK; (**b**) Particle morphology of PEEK/CF_30wt%.

Table 3. Average particle size distribution range of PEEK and CF.

Material	Particle size (μm)	
	PEEK	CF
D_{10}	23.884	6.39
D_{50}	46.702	13.433
D_{90}	84.546	77.043

Preprints (www.preprints.org) | NOT PEER-REVIEWED | Posted: 8 June 2023 doi:10.20944/preprints202306.0607.v1

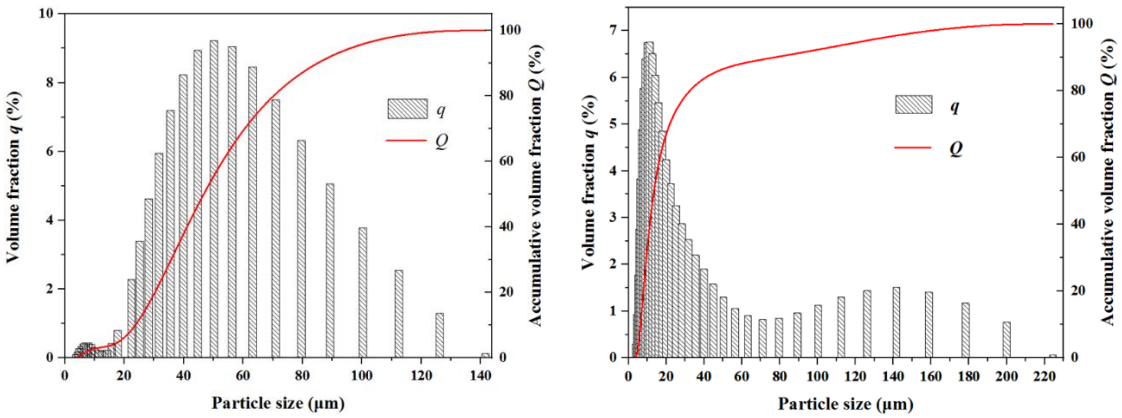

Figure 9. Particle size distribution: (**a**) PEEK; (**b**) CF.

It shows that the average particle size of PEEK is larger than that of CF. The majority of PEEK particles are in the range of 30-60 μm while the lengths of numerous CF particles are scoped by 5-20 μm.

The restitution coefficient and the static friction coefficient are directly acquired according to the finite element simulation and inclined plane test respectively. The corresponding results are summarized in Table 4. It appears that the PEEK-related static friction coefficients reach higher values compared with the CF-CF, which is caused by the irregular shapes and unsmooth surface property of the PEEK particles. The glass-related static friction coefficients are minimum due to the glossy surface. As for the restitution coefficient, the PEEK particles possess good elasticity inducing the PEEK-related restitution coefficients to present larger values than the CF-related restitution coefficients.

Table 4. The results of the restitution coefficient and the static friction coefficient.

Type	Static friction coefficient				Restitution coefficient		
	Tilt angle $\alpha 1$ (°)	Tilt angle $\alpha 2$ (°)	Tilt angle $\alpha 3$ (°)	μ	v_{app}[1] (m/s)	v_{off} (m/s)	e
CF-PEEK	25.34	24.92	25.62	0.4726	1.98	0.5336	0.2695
CF-CF	21.18	20.41	21.33	0.3833	1.98	0.1665	0.0841
PEEK-PEEK	25.13	25.42	24.82	0.4689	1.98	0.5437	0.2746
CF-glass	5.89	5.91	5.70	0.1021	1.98	0.1677	0.0847
PEEK-glass	8.20	8.34	7.85	0.1429	1.98	0.5405	0.2730

[1] Elastic modulus of CF is 15Gpa along the horizontal direction.

The bulk density results of PEEK and PEEK/CF powders are shown in Table 5. It is observed that the bulk density of PEEK/CF is higher than that of the PEEK powder, and the bulk density of PEEK/CF increases with the increase of the CF mass fraction. Because the solid-phase density of CF is slightly higher than that of the PEEK, and most CF particles have smaller sizes, filling the pores between PEEK particles.

Table 5. The bulk density results of PEEK and PEEK/CF.

Powder	Empty graduated cylinder (g)	Full graduated cylinder (g)	volume (ml)	Bulk density (g·cm^{-3})
PEEK	50.9169	92.4863	100	0.4157
PEEK/CF_30wt%	51.5233	102.9567	100	0.5143
PEEK/CF_50wt%	51.6115	107.061	100	0.5545

Preprints (www.preprints.org) | NOT PEER-REVIEWED | Posted: 8 June 2023 doi:10.20944/preprints202306.0607.v1

4.2 Results of DOE

The rolling friction coefficient and surface energy can not be directly measured through experimental methods, so the "PB-BBD-GA" method is used to acquire the optimal combination of rolling friction coefficient and surface energy. Therein, the PB design aims to determine the significant parameters of related rolling friction coefficient and surface energy. Detailed design and response results of the PB test are listed in Table 6. The significance analysis of the model and corresponding factors is given in Table 7.

Table 6. The design and results of the PB test.

No.	Rolling friction coefficient					Surface energy			Virtual parameters			AOR(°)
	X_0	X_1	X_2	X_3	X_4	X_5	X_6	X_7	*A*	*B*	*C*	
1	0.20	0.20	0.01	0.20	0.20	0.02	0.001	0.001	-1	1	-1	48.92
2	0.01	0.20	0.20	0.01	0.20	0.02	0.02	0.001	-1	-1	1	45.30
3	0.20	0.01	0.20	0.20	0.01	0.02	0.02	0.02	-1	-1	-1	46.90
4	0.01	0.20	0.01	0.20	0.20	0.001	0.02	0.02	1	-1	-1	38.62
5	0.01	0.01	0.20	0.01	0.20	0.02	0.001	0.02	1	1	-1	33.74
6	0.01	0.01	0.01	0.20	0.01	0.02	0.02	0.001	1	1	1	33.75
7	0.20	0.01	0.01	0.01	0.20	0.001	0.02	0.02	-1	1	1	42.17
8	0.20	0.20	0.01	0.01	0.01	0.02	0.001	0.02	1	-1	1	48.48
9	0.20	0.20	0.20	0.01	0.01	0.001	0.02	0.001	1	1	-1	45.81
10	0.01	0.20	0.20	0.20	0.01	0.001	0.001	0.02	-1	1	1	38.23
11	0.20	0.01	0.20	0.20	0.20	0.001	0.001	0.001	1	-1	1	42.54
12	0.01	0.01	0.01	0.01	0.01	0.001	0.001	0.001	-1	-1	-1	26.10

Table 7. Significance analysis of the model and corresponding parameters of the PB test.

Source	Sum of squares	df	Mean square	F-value	P-value	
Model	526.34	8	65.79	15.01	0.0239	significant
X_0	290.94	1	290.94	66.36	0.0039	significant
X_1	134.44	1	134.44	30.66	0.0116	significant
X_2	17.43	1	17.43	3.98	0.1401	-
X_3	4.53	1	4.53	1.03	0.3843	-
X_4	12.04	1	12.04	2.75	0.1961	-
X_5	46.55	1	46.55	10.62	0.0472	significant
X_6	17.67	1	17.67	4.03	0.1383	-
X_7	2.74	1	2.74	0.6253	0.4868	-
R^2=0.9756, Adjusted R^2=0.9106						

As shown in Table 7, both R2 and Adjusted-R2 are close to 1, which means that the model and the chosen response value of AOR are reasonable. The significance can be

Preprints (www.preprints.org) | NOT PEER-REVIEWED | Posted: 8 June 2023 doi:10.20944/preprints202306.0607.v1

reflected by the P-value. The p-value less than 0.05 correlates with the significant factor. Therefore, the parameters of PEEK-PEEK rolling friction coefficient (X0), PEEK-CF rolling friction coefficient (X1), and PEEK-PEEK surface energy (X5) have significant effects on the AOR. Among them, the influence of X0, X1, and X5 are in descending order, which can be obtained through the F-value. This indicates that the effect of the rolling friction coefficient is greater than that of surface energy in this work. Since the ellipsoidal particles of PEEK are replaced by round particles, the rolling friction coefficient should be utilized to make up for the shape approximation in the powder dynamics simulation. Analogous treatment is also found in the literature of [36, 37]. Regarding the parameter of rolling friction coefficient/surface energy, the general influence order of PEEK-PEEK, PEEK-CF, and CF-CF is in descending trend, which means that the interaction between CF particles is minimally effective in the composite powders PEEK/CF.

Since the significant parameters (X0, X1, X5) are determined by the PB test, the remaining insignificant parameters can be reasonably fixed before the BBD design. The parameters of X2, X3, and X4 are fixed as 0.01, X6 and X7 are set to 0.001. Sequentially, the detailed BBD design (correlated with the parameters of X0, X1, and X5) and response-value of AOR are listed in Table 8. The variance analysis of the whole model and the corresponding factors are given in the following Table 9. Herein, the insignificant quadratic and cross-terms are eliminated for the convenience of analysis and subsequent calculation. The P-value of the model is extremely small, which shows that the entire model is reliable and the AOR can be reasonably predicted. Interestingly, the significance of cross-terms is greater than that of the quadratic term (eliminated here) in this numerical example.

Table 8. The design and results of the BBD test.

No.	X_0	X_1	X_5	AOR (°)
1	0.010	0.010	0.0105	24.21
2	0.200	0.010	0.0105	37.33
3	0.010	0.200	0.0105	37.56
4	0.200	0.200	0.0105	40.82
5	0.010	0.155	0.0010	30.29
6	0.200	0.155	0.0010	41.53
7	0.010	0.155	0.020	31.11
8	0.200	0.155	0.020	42.83
9	0.105	0.010	0.001	28.40
10	0.105	0.200	0.001	40.52
11	0.105	0.010	0.020	32.41
12	0.105	0.200	0.020	38.19
13	0.105	0.105	0.0105	34.95

Table 9. Significance analysis of the model and corresponding parameters of BBD test.

Source	Sum of squares	df	Mean square	F-value	P-value	
Model	380.53	5	76.11	66.39	7.68E-08	significant
X_0	193.51	1	193.51	168.81	5.12E-08	significant
X_1	150.82	1	150.82	131.57	1.85E-07	significant
X_5	1.81	1	1.81	1.57	0.235541	-

Preprints (www.preprints.org) | NOT PEER-REVIEWED | Posted: 8 June 2023 doi:10.20944/preprints202306.0607.v1

X_0X_1	24.34	1	24.34	21.24	0.000755	significant
X_1X_5	10.05	1	10.05	8.77	0.012946	significant

R^2=0.9679, Adjusted R^2=0.9533

Based on the results of the BBD design, the quadratic regression model for the response value (AOR) and the investigated variables (X0, X1, X5) can be established as:

$$ROE_{real}=20.17425+52.10569X_0+60.21470X_1+228.37659X_5 -117.3365X_0X_1-1150.8167X_1X_5 \quad (0.01 \le X_0 \le 0.2,\ 0.01 \le X_1 \le 0.2,\ 0.001 \le X_5 \le 0.02) \tag{25}$$

$$ROE_{cod}=35.29+4.92A+4.34B+0.475C-2.47AB-1.59BC \quad (A,B,C \in [-1,1]) \tag{26}$$

Therein, Eq. (25) is in terms of the actual factors and can be utilized to predict the AOR. Eq. (26) is in terms of the coded factors, which is necessary for the subsequent GA. In Eq. (26), the term A corresponds to X0, B corresponds to X1, and C corresponds to X5. The upper (-1) and lower limits (1) of the value range of term A correlated with the upper (0.01) and lower limits (0.2) of factor X0, which is also correspondingly applied for the terms B and C.

When the predictive equation of AOR is acquired based on the BBD design, the corresponding optimal parameters of rolling friction coefficient and surface energy can be achieved by making the predicted AOR equal to the experimental value (34.23° for the PEEK/CF_30wt%). Thus, the objective equation for the GA is expressed as

$$\left(ROE_{cod}-34.23\right)^2=0 \tag{27}$$

Eq. (27) is input into the MATLAB GA toolbox with the value range of [-1,1] for all corresponding variables. The results are given in Table 10. So far, all the essential factors have been determined for the powder dynamics model.

Table 10. The optimal parameters obtained by the GA.

Variable		Coded value			Real value
Coded	Real	Max	Min	Optimal	
A	X_0	1	-1	-0.169	0.1305
B	X_1	1	-1	0.008	0.1562
C	X_5	1	-1	-0.581	0.0050

4.3 Experimental verification

The calibrated DEM model for the PEEK/CF composite powders should be experimentally verified. As a comprehensive index of powder properties, AOR can be utilized to conduct the experimental verification work. The AOR experiment is carried out based on the standard GB11986-89. The Experimental AOR results of PEEK, PEEK/CF_30wt%, and PEEK/CF_50wt% are shown in Figure 10(a), with the detailed data listed in Table 11. The simulation results are shown in Figure 10(b), and the detailed data are given in Table 12. It appears that the experimental and simulation results show a maximal variance of 4.89 %, which can indicate the high reliability and effectiveness of the developed powder dynamics model.

Preprints (www.preprints.org) | NOT PEER-REVIEWED | Posted: 8 June 2023 doi:10.20944/preprints202306.0607.v1

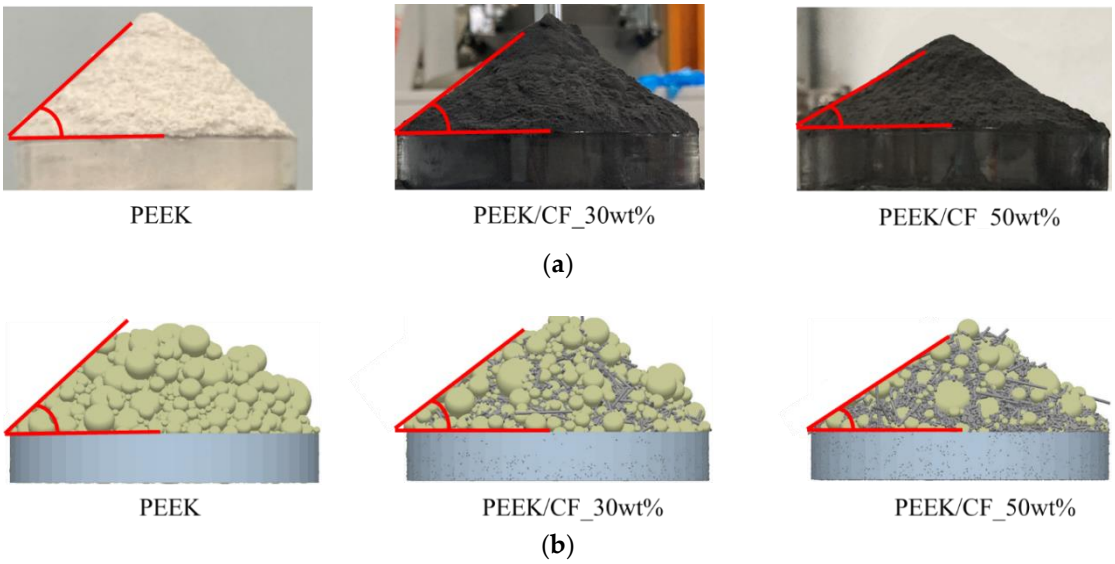

Figure 10. The experimental and simulation results of AORs for PEEK, PEEK/CF_30wt%, and PEEK/CF_50wt%: (**a**) Experimental results; (**b**) Simulation results.

Table 11. Experimental AORs of PEEK, PEEK/CF_30wt%, and PEEK/CF_50wt%.

Powder	Repose angle θ (°)			
	Group1	Group2	Group3	Average
PEEK	41.59	41.43	41.65	41.56
PEEK/CF_30wt%[1]	33.66	34.86	34.17	34.23
PEEK/CF_50wt%	28.29	27.93	27.37	27.86

[1] The AOR of PEEK/CF_30wt% has been referenced at the DOE process, thus the AORs of PEEK/CF_50wt% and PEEK are the verification targets.

It also reveals that the pure PEEK possesses the largest AOR, which implies the minimum of powder fluidity. With the addition of CF, the AOR of the composite powder decreases and the powder fluidity rises. Importantly, the AOR decreases with the increase of the weight fraction of CF, exhibiting improved powder fluidity. Since the powder fluidity is greatly affected by the cohesive effect between particles of PEEK-PEEK, PEEK-CF, and CF-CF. The influence of PEEK-PEEK, PEEK-CF, and CF-CF interfacial reactions on the composite AOR is in descending order (discussed in Section 4.2). The PEEK-related cohesion plays a dominant role in the PEEK/CF powder packing. Thus, the increased volume fraction of CF leads to the decrease of total cohesive interaction between particles, resulting in improved powder fluidity.

Table 12. The comparison between simulation and experimental results of AOR.

Material	Simulation results of AOR (°)					Experimental AOR (°)	Error (%)
	x+*	*x*-*	*y*+*	*y*-*	Average		
PEEK	44.54	43.70	41.98	43.11	43.33	41.56	4.26
PEEK/CF_30wt%	36.29	35.01	36.48	35.84	35.90	34.23	4.89
PEEK/CF_50wt%	25.46	29.37	28.36	28.81	28.00	27.86	0.50

[1] *x*+, *x*-, *y*+, and *y*- represent the directions when reading the AOR results.

4.4 Evaluation of the powder deposition

The investigation of the powder deposition process is necessary to achieve the expected behaviors of the laser-sintered parts in PEEK/CF composites. The surface properties and recoating difficulty of powder layers can be evaluated in a qualitative fashion by the powder deposition process. Figure 11 shows the micro-pictures of the surface

Preprints (www.preprints.org) | NOT PEER-REVIEWED | Posted: 8 June 2023 doi:10.20944/preprints202306.0607.v1

topography and undulation of PEEK, PEEK/CF_30wt%, and PEEK/CF_50wt%. It appears that the image quality of the surface morphology of PEEK is worse than the other two composite powders. This indicates a violent surface fluctuation of the PEEK powders, which is caused by the inhomogeneous particle distribution-induced porosity. With the addition of the CF, the surface quality is improved and also meliorates with the increase of the weight fraction of CF, which is caused by the particle distribution of the adopted CF. As shown in Figure 9(b), numerous CF particles exhibit the size range of 5-20 μm. These small and uneven CF particles exactly fill the inter-particle cavity among PEEK powders, and the surface of its powder bed is observed smoothly.

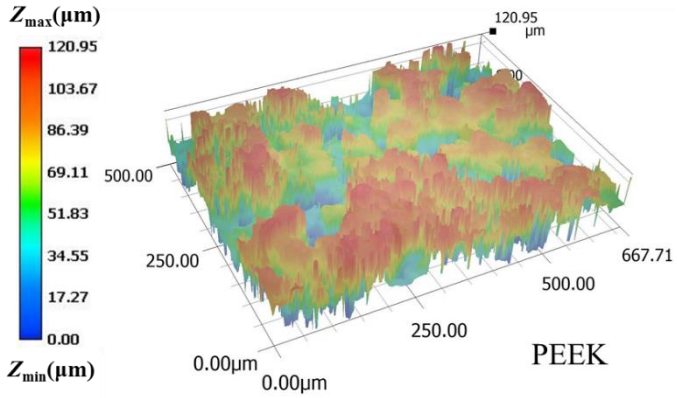

(a)

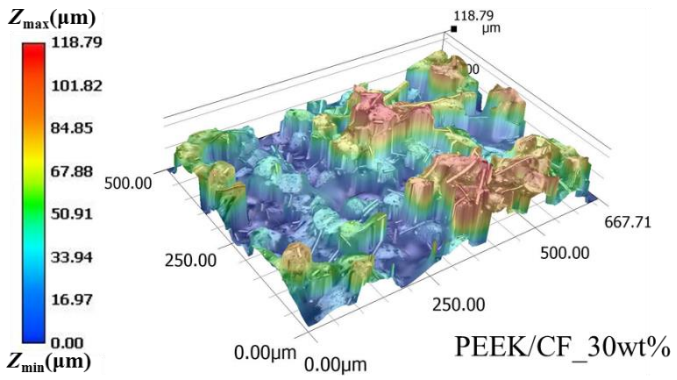

(b)

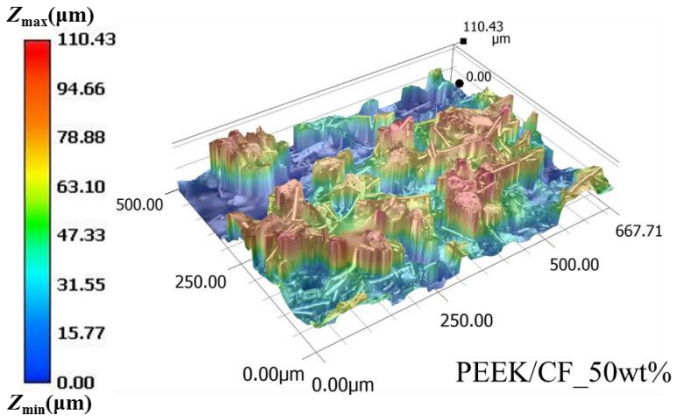

(c)

Figure 11. The experimental micro-pictures of the surface topography and undulation: (**a**) PEEK; (**b**) PEEK/CF_30wt%; (**c**) PEEK/CF_50wt%.

Preprints (www.preprints.org) | NOT PEER-REVIEWED | Posted: 8 June 2023 doi:10.20944/preprints202306.0607.v1

Figure 12 shows the cross-sections of the simulated powder deposition results. It also shows that drastic undulation occurs on the PEEK surface. The surface fluctuation of PEEK/CF_30wt% is slightly mitigated and improved a lot for the PEEK/CF_50wt%, which is consistent with the experimental results. The standard deviation of the surface contour curve of the powder deposition layer is used to quantitatively characterize the fluctuation of the layer surface. The fluctuation of the layer surface decreases with the decrease of the standard deviation, and the corresponding powder layer becomes smoother.

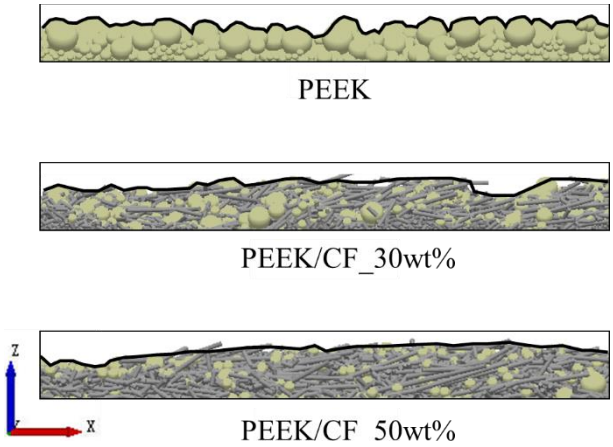

Figure 12. The cross-section of the simulated powder deposition of PEEK, PEEK/CF_30wt%, and PEEK/CF_50wt%.

The experimental and simulation results of the standard deviation of the surface contour curve are shown in Figure 13 and Table 13. According to the experimental results, the surface smoothness of PEEK/CF_30wt% is increased by 31.3% compared to the PEEK powder, while the surface smoothness of PEEK/CF_50wt% powder is improved by 55.2% compared to PEEK powder. According to the simulation results, compared to the PEEK powder, the surface smoothness of the PEEK/CF_30wt% is increased by 27.4%, and 50.2% improved of the PEEK/CF_50wt% powder. The similar results of experimental and simulation further verifies the reliability of the DEM model.

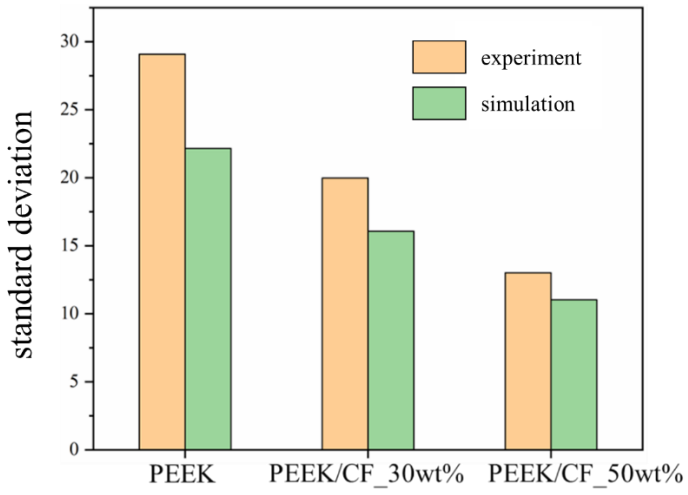

Figure 13. Experimental and simulation results of standard deviation of powder surface profile.

Table 13. Experimental and simulation results of the improvement of PEEK/CF_30wt% and PEEK/CF_50wt% compared to PEEK.

Powder	Standard deviation of the surface contour curve

Preprints (www.preprints.org) | NOT PEER-REVIEWED | Posted: 8 June 2023 doi:10.20944/preprints202306.0607.v1

	experiment	Improvement compared to PEEK	Simulation	Improvement compared to PEEK
PEEK	29.07	-	22.15	-
PEEK/CF_30wt%	19.98	31.3% ↑	16.07	27.4% ↑
PEEK/CF_50wt%	13.01	55.2% ↑	11.02	50.2% ↑

In summary, the method of systematic material evaluation possesses universal applicability for different types of composite powders even multi-component composites. The powder dynamic modeling for composite powders has been developed to well simulate the composite powder deposition. The deposition parameters can be optimized using the DEM approach effectively.

5. Conclusions

This work proposes a systematic framework for material evaluation to incorporate with powder dynamics model for numerical investigation of composite powder deposition. PEEK/CF as typical feedstock materials of laser sintering are investigated, and the interaction of short CF and PEEK powders are quantified upon deposition. It shows that the AOR decreases with the increase of the weight fraction of CF. This indicates the improved powder fluidity with the addition of a proper percentage of CF with the length in 5-20 μm. The surface quality is also improved with the increase of the weight fraction of CF.

Importantly, this method is generally applicable to investigate the dynamic behaviors of different types of composite powders including multi-component particles. The developed deposition model can be helpful to optimize the deposition parameters and material composition so as to improve the packing quality of composite powders, which significantly influences the PBF process of composite materials in additive manufacturing.

Author Contributions: Conceptualization, J.L. and F.P.; methodology, J.L.; software, J.L. and H.L.; validation, J.L., Z.R. and J.F.; formal analysis, W.Z.; investigation, J.L.; resources, F.P.; data curation, H.L. and Z.R.; writing—original draft preparation, J.L.; writing—review and editing, J.L. and J.F.; visualization, J.L.; supervision, F.P. All authors have read and agreed to the published version of the manuscript.

Funding: This research received no external funding.

Conflicts of Interest: The authors declare that they have no known competing financial interests or personal relationships that could have appeared to influence the work reported in this paper.

References

1. S. Yuan, S. Li, J. Zhu, Y. Tang, Additive manufacturing of polymeric composites from material processing to structural design, *Composites Part B: Engineering*, 219 (2021) 108903.
2. Hui Chen Y C, Yin Liu, Qingsong Wei, Yusheng Shi, Wentao Yan*, Packing quality of powder layer during counter-rolling-type powder spreading process in additive manufacturing, *International Journal of Machine Tools and Manufacture*, 153 (2020) 103553.
3. W. Nan, M. Pasha, M. Ghadiri, Numerical simulation of particle flow and segregation during roller spreading process in additive manufacturing, *Powder Technology*, **2020**, 364, 811-821.
4. A. Campos, O. Oliveira, L. Ferreira, M. Francisquetti, M. Barrozo, K. Santos, Dem simulations of dynamic angle of repose of acerola residue: a parametric study using a response surface technique, **2014**.
5. F. Lv, X. Wang, M. Zhang, H. Fu, J. Yu, Determination and Analysis for Parameters of Shape, Size, Physical and Mechanical Properties of Soybean Grains, in: X. Li, Y. Feng, G. Mustoe (Eds.) *Proceedings of the 7th International Conference on Discrete Element Methods*, Springer Singapore, **2017**, 1277-1286.
6. J. Horabik, M. Beczek, R. Mazur, P. Parafiniuk, M. Ryżak, M. Molenda, Determination of the restitution coefficient of seeds and coefficients of visco-elastic Hertz contact models for DEM simulations, *Biosystems Engineering*, **2017**, 161, 106-119.
7. N. Belheine, J.P. Plassiard, F.V. Donzé, F. Darve, A. Seridi, Numerical simulation of drained triaxial test using 3D discrete element modeling, *Computers and Geotechnics*, **2009**, 36, 320-331.
8. M. Ucgul, J.M. Fielke, C. Saunders, Three-dimensional discrete element modelling of tillage: Determination of a suitable contact model and parameters for a cohesionless soil, *Biosystems Engineering*, **2014**, 121, 105-117.

 doi:10.20944/preprints202306.0607.v1

9. J. Yoon, Application of experimental design and optimization to PFC model calibration in uniaxial compression simulation, *International Journal of Rock Mechanics and Mining Sciences*, **2007**, 44, 871-889.
10. H. Shimizu, T. Koyama, T. Ishida, M. Chijimatsu, T. Fujita, S. Nakama, Distinct element analysis for Class II behavior of rocks under uniaxial compression, *International Journal of Rock Mechanics and Mining Sciences*, **2010**, 47 323-333.
11. M. Sagong, D. Park, J. Yoo, J.S. Lee, Experimental and numerical analyses of an opening in a jointed rock mass under biaxial compression, *International Journal of Rock Mechanics and Mining Sciences*, **2011**, 48 1055-1067.
12. L. Vu-Quoc, X. Zhang, O.R. Walton, A 3-D discrete-element method for dry granular flows of ellipsoidal particles, *Computer Methods in Applied Mechanics and Engineering*, **2000**, 187, 483-528.
13. I. Marczewska, J. Rojek, R. Kačianauskas, Investigation of the effective elastic parameters in the discrete element model of granular material by the triaxial compression test, *Archives of Civil and Mechanical Engineering*, **2016**, 16, 64-75.
14. M.W. Johnstone, Calibration of DEM models for granular materials using bulk physical tests, **2010**.
15. E.X. Zu, P. Zhou, Z.H. Jiang, Discrete Element Method of Coke Accumulation: Calibration of the Contact Parameter, *IFAC-PapersOnLine*, **2018**, 51, 241-245.
16. G.D. C. Thornton, Contact Mechanics and Particle System Simulations: A DEM study, **2015**.
17. P.A. Cundall, O.D.L. Strack, A discrete numerical model for granular assemblies, *Géotechnique*, **1979**, 29, 47-65.
18. H.P. Zhu, Z.Y. Zhou, R.Y. Yang, A.B. Yu, Discrete particle simulation of particulate systems: Theoretical developments, *Chemical Engineering Science*, **2007**, 62, 3378-3396.
19. Q. Li, V. Rudolph, B. Weigl, A. Earl, Interparticle van der Waals force in powder flowability and compactibility, *International Journal of Pharmaceutics*, **2004**, 280, 77-93.
20. A. Di Renzo, F.P. Di Maio, Comparison of contact-force models for the simulation of collisions in DEM-based granular flow codes, *Chemical Engineering Science*, **2004**, 59, 525-541.
21. W. Yan, Y. Qian, W. Ge, S. Lin, W.K. Liu, F. Lin, G.J. Wagner, Meso-scale modeling of multiple-layer fabrication process in Selective Electron Beam Melting: Inter-layer/track voids formation, *Materials & Design*, **2018**, 14, 210-219.
22. K.L. Johnson, I. Sridhar, Adhesion between a spherical indenter and an elastic solid with a compliant elastic coating, *Journal of Physics D: Applied Physics*, **2001**, 34, 683.
23. M. R, Elastic Spheres in Contact Under Varying Oblique Forces, *J Applied Mechanics*, **1949**, 16(7), 327-330.
24. H. H, On the contact of elastic solids, *Journal für die reine und angewandte Mathematik (Crelles Journal)*, **1882**, 92, 156-171.
25. Y. Tsuji, T. Tanaka, T. Ishida, Lagrangian numerical simulation of plug flow of cohesionless particles in a horizontal pipe, *Powder Technology*, **1992**, 71, 239-250.
26. O.E. Sakaguchi H, Igarashi T, Plugging of the flow of granular materials during the discharge from a silo, *International Journal of Modern Physics B*, **1993**, 7(10), 1949-1963.
27. K.K. Johnson K L, Roberts A, Surface energy and the contact of elastic solids, *Proceedings of the royal society of London A mathematical and physical sciences*, **1971**, 324(1558), 301-313.
28. W. Nan, Y. Wang, H. Tang, A viscoelastic model for flexible fibers with material damping, *Powder Technology*, **2015**, 276, 175-182.
29. A. Katterfeld, C.J. Coetzee, T. Donohue, J. Fottner, A. Grima, Á. Ramírez-Gómez, D. Ilic, R. Kačianauskas, J. Necas, D. Schott, K. Williams, J. Zegzulka, Calibration of DEM Parameters for Cohesionless Bulk Materials under Rapid Flow Conditions and Low Consolidation, **2019**.
30. H. Chen, Y. Sun, W. Yuan, S. Pang, W. Yan, Y. Shi, A Review on Discrete Element Method Simulation in Laser Powder Bed Fusion Additive Manufacturing, *Chinese Journal of Mechanical Engineering: Additive Manufacturing Frontiers*, **2022**, 1, 100017.
31. D. Garcia-Gonzalez, A. Rusinek, T. Jankowiak, A. Arias, Mechanical impact behavior of polyether–ether–ketone (PEEK), *Composite Structures*, **2015**, 124, 88-99.
32. X. Chao, L. Qi, W. Tian, Y. Lu, H. Li, Potential of porous pyrolytic carbon for producing zero thermal expansion coefficient composites: A multi-scale numerical evaluation, *Composite Structures*, **2020**, 235, 111819.
33. Z.H.J. T. Ge, K.D. Zhou, A Theoretical Model for the Coefficient of Restitution Calculation of Point Impact, *Machine Design & Research*, **2007**.
34. Abaqus Analysis User's Guide,Dassault Systèmes Simulia Corp, **2017**, 23(3), 14-15.
35. Optimization of alkaline protease production by batch culture of Bacillus sp. RKY3 through Plackett-Burman and response surface methodological approaches, *Bioresource Technology*, **2008**.
36. H. Zhou, Z. Hu, J. Chen, X. Lv, N. Xie, Calibration of DEM models for irregular particles based on experimental design method and bulk experiments, *Powder Technology*, **2018**, 332, 210-223.
37. Y.C. Zhou, B.D. Wright, R.Y. Yang, B.H. Xu, A.B. Yu, Rolling friction in the dynamic simulation of sandpile formation, *Physica A: Statistical Mechanics and its Applications*, **1999**, 269, 536-553.